Available online at www.sciencedirect.com
SCIENCE DIRECT®
ELSEVIER
International Journal of Solids and Structures 41 (2004) 6699–6724
INTERNATIONAL JOURNAL OF SOLIDS and STRUCTURES
www.elsevier.com/locate/ijsolstr

An experimental study of pre-notched clamped beams under impact loading

F.L. Chen [a,b,*], T.X. Yu [b]

[a] Institute of Applied Physics and Computational Mathematics, P.O. Box 8009-11, Beijing 100088, PR China
[b] Department of Mechanical Engineering, Hong Kong University of Science and Technology, Clear Water Bay, Kowloon, Hong Kong

Received 14 May 2004
Available online 20 July 2004

Abstract

Experiments were conducted aiming to systematically investigate the failure behavior of clamped beams with one pre-notch or two pre-notches under impact loading from a projectile strike. High-speed digital video photography was successfully applied in the structural impact tests to record in real time the hasty scenario of the specimens' deformations and failures. It is observed that even a minor pre-notch in a beam may dramatically alter its dynamic response and failure behavior by making it much easier to break. That is, with the presence of pre-notches, the beam' dynamic response pattern would switch from a large global ductile plastic deformation to a local strength-failure, which evolves from crack initiation and extension to a breakage. In this case, much more plastic dissipation is localized at the pre-notched cross-section(s) and the breakage is caused basically by a Mode I crack extension. The effect of pre-notch is found to be strongly location-dependent and surface-dependent.

Keywords: Pre-notch; Clamped beam; Impact loading; Dynamic response and failure

1. Introduction

Collisions and dynamic loads very often play an important role in a wide variety of engineering structural failures. Different failure modes may develop in a structure under various dynamic loading conditions. Menkes and Opat (1973) conducted an experimental investigation into the dynamic plastic response and failure of fully clamped metal beams subjected to uniformly distributed velocities over the entire span. They identified three basic failure modes for impulsively loaded fully clamped beams: large inelastic deformation (failure mode I), tensile tearing (failure mode II) and transverse shear failure at the supports (failure mode III). The failure of fully clamped beams struck by a mass was then examined by Liu and Jones (1987), Jones (1989) and Yu and Jones (1991), who observed that for sufficiently large impact

* Corresponding author. Current address: Institute of Applied Physics and Computational Mathematics, P.O. Box 8009-11, Beijing 100088, PR China. Tel.: +86-10-62014411; fax: +86-10-62010108.
E-mail address: flchen@iapcm.ac.cn (F.L. Chen).

0020-7683/$ see front matter © 2004 Elsevier Ltd. All rights reserved.
doi:10.1016/j.ijsolstr.2004.05.036

Nomenclature

$\bar{a}$	average deceleration of projectile from 0 to t_s, V_0/t_s
B	breadth of beam
C	depth of pre-notch
E	Young's modulus
E_p	hardening modulus
$\overline{F}$	average impact force, $G\bar{a}$
G	mass of projectile
β	mass ratio, $G/(2\rho BHL)$
H	thickness of beam
I_0	momentum of projectile, GV_0
K_r	kinetic energy taken away by rebounded projectile, $GV_r^2/2$
K_0	kinetic energy of projectile before impact, $GV_0^2/2$
L	half effective length of beam
M_0	fully plastic bending moment of perfect beam, $YBH^2/4$
P	air pressure in gun chamber
R	energy ratio, K_0/U_{max}^e
t	time
t_b	time when beam breaks or an obvious crack appears
t_s	time when projectile stops going ahead
t_r	time when projectile separates from beam
U_{max}^e	maximum elastic energy that the beam can store, $M_0^2(2L)/2EI$
V_c	critical impact velocity
V_r	rebounding velocity of projectile
V_0	projectile velocity just before impact
w	width of pre-notch
W_{max}	maximum deflection of beam
Y	yield stress
v	Poisson's ratio
ρ	density of beam
σ_p	peak stress of beam material
γ	reduced factor on fully plastic bending moment due to pre-notch, $(1 - C/H)^2$
θ_f	rotation angle at pre-notched section after impact

energies, the tested beams were broken or cracked at the impact point with a shear mode, which is referred as failure mode IV by Yu and Chen (2000a).

Despite the very limited experimental investigations, numerous theoretical and numerical works have been published to study the dynamic failure of beams, such as Nonaka (1967), Jones (1976), Liu and Jones (1988), Shen and Jones (1993), Yu and Jones (1997), Yu and Chen (2000b), and Li and Jones (2000), etc. They provided theoretical predictions on the threshold impact energy for the onset of different failure modes of beams by employing various failure criteria. However, in order to observe a structure's basic failure modes and to verify the predictions obtained from theoretical analyses and finite element simulations, and/or to acquire evidence to refine the relevant theories, experimental studies remain of essential importance.

While most of the previous studies in the field of structural impact are restricted to uniform and perfect structural members, real structures are usually "imperfect" in their geometry; for example, they may contain notches, cracks or defects on their cross-sections. Engineering practice indicates that imperfect or defected sections in a structure will trap a significant part of the work done by dynamic loads and thereby alter the dynamic failure features of the structure. There have been so far only a few experimental works reported in the literature which dealt with notched (imperfect) simple structural members, including notched free–free beams (Woodward and Baxter, 1986), notched cantilevers (Petroski and Verma, 1985), and symmetrically notched circular rings (Zhao et al., 1995). The structures tested in these three sets of experiments possessed weaker constraints at their ends, so that bending moment acted as the sole structural internal force of significance. Yang et al. (1992) conducted an experiment on notched clamped beams subjected to impact, but only ductile plastic deformation (no strength failure) was observed and measured in the experiment. In addition, owing to a limited amount of specimens tested in all these experiments, only fragmentary information has been gained. For example, almost no real-time experimental evidence, especially no quantitative data on the threshold impact energy, that a notched specimen can withstand, has been acquired.

A set of comprehensive impact experiments was recently conducted by the authors to investigate the failure behaviors (e.g. crack initiation and extension, as well as breakage) of clamped beams with pre-notch under impact of a projectile strike. In particular, an advanced experimental technology—high-speed digital video photography—was successfully applied in the structural impact tests to record in real-time the hastily changing scenario of the specimens' deformation and failure. This paper presents the major experimental results and discusses the pre-notched beams' failure characteristics, especially the failure threshold of pre-notched beams subjected to projectile impact.

2. Experimental set-up and material test

2.1. Experimental set-up

The experiments were conducted using an Air Gun Testing System (AGTS). As shown in Fig. 1, the AGTS is composed of four components: (i) a major part consisting of a compressed air source with pressure up to 10 MPa, a gun chamber, a 14.5 mm gun barrel, and a projectile, etc.; (ii) a control panel; (iii) a target area consisting of specimens, a supporting frame and a safeguard shelter; and (iv) a measurement system, e.g. a velocity measurement sub-system and photography, diagnostics, recording and data processing instruments, etc.

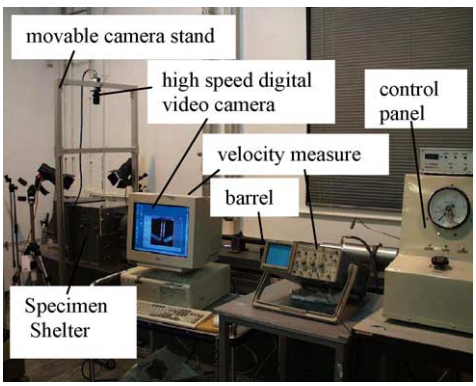

Fig. 1. Air Gun Testing System (AGTS) and experimental set-up with the high-speed video photography technology being used.

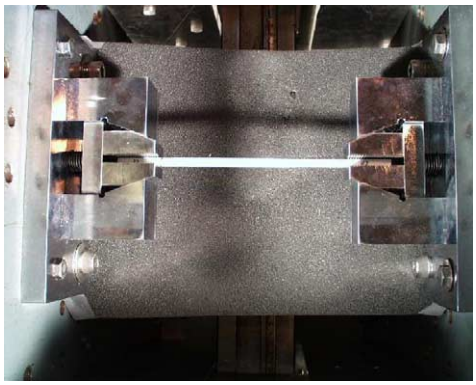

Fig. 2. Specially designed supporting frame and fixtures with a self-lock mechanism.

A pair of specially designed fixtures (Fig. 2) was machined to achieve the expected supporting condition. This fixture contained a smart self-lock mechanism that ensures the specimen being clamped tightly during the deformation process; and it facilitated convenient mounting and dismantling of the specimen. With the specifically designed mechanism, the specimens were held quite firmly by the fixtures and could be approximately regarded as fully clamped since only a trivial relative axial movement was observed thereof in each test. The front and top covers of the target area shelter were made of transparent plexiglass, allowing one to observe the deforming specimen from the front and to shoot high-speed photographs from the top. The velocity measurement system for the projectile consisted of two SUNX photoelectric infrared sensors and a Tektronix 2212 60 MHz digital storage oscilloscope.

Dynamic response and failure of a structural specimen under impact is an extremely swift process, usually lasting only a few milliseconds. In general, it is very difficult to conduct real-time measurements in such a hasty testing process. However, for a better understanding of the complicated phenomena and the associated mechanical mechanism, real-time experimental evidences are indeed precious. In our tests, we successfully used the high-speed digital video camera (recording rate: 60–8000 frames/s; sensor resolution: 480 420 to 60 68) to record the rapid change of the specimens' deformation and failure scenarios, which generated movies in the .avi format or frames of photographs in the .bmp format that can be shown on a PC screen (see Fig. 1). This could be the first time that this state-of-the-art digital experimental technology was used in a structural impact experiment.

2.2. Projectiles and specimens

Three types of cylindrical projectiles, shown in Fig. 3, were used in the tests. They were made of aluminium (labelled by A1a, A1b or A1c), steel (S1b, S1c) or high-density steel (HS1a), whose specifications are given in Table 1.

All the beam specimens were made of Aluminium 6061 T6, which is widely regarded as a strain-rate insensitive material. The dimensions of the beam specimens were 6.35 mm(B) 6.35 mm(H) 210.0 mm each, with effective length $2L = 142.0$ mm when mounted onto the supporting frame by the fixtures.

Except for a few perfect specimens (not pre-notched), most of beam specimens were machined to have one pre-notch or two pre-notches by use of a milling machine. The over 60 specimens were divided into four groups in terms of the notch details, attempting to examine the effects of various factors, e.g. the effect of notch's presence (notch depth: 0, $0.13H$, $H/4$ and $H/3$), the effect of notch location (at $0L$, $L/4$, $L/2$, $3L/4$ and L), the influence of notch width/tip sharpness (1.5, 0.8, 0.5 and 0.9 mm plus a sharp tip of angle 45°, refer to Fig. 4), and how a notched beam behaves differently with increasing impact velocity (ranged from 10 to 60 m/s).

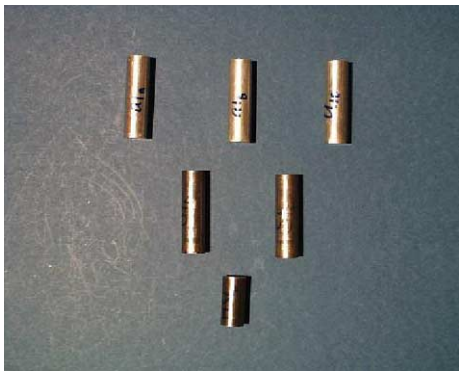

Fig. 3. Three types of projectiles.

Table 1
Specifications of projectiles used

Projectile no.	Diameter (mm)	Length (mm)	Mass G (g)
A1a, A1b, A1c	14.45	50.00	22.8
S1b, S1c	14.45	50.00	64.0
HS1a	14.45	29.10	84.5

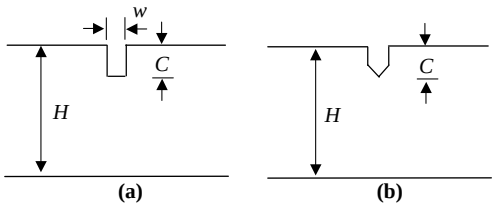

Fig. 4. Schematic of pre-notches: (a) Π-shaped and (b) with sharp tip. H: thickness of beam, C: notch depth and w: notch width.

2.3. Mechanical properties of specimen material

Both uni-axial tensile and three point bending tests were carried out, using a Sintech MTS D/10 Universal Testing Machine and a MTS 858 UTM, respectively, to quantify the mechanical properties of the beam material, ALCOA aluminium 6061 T6. The simple tensile and three-point bending diagrams for samples made of the same material are depicted in Fig. 5(a) and (b), respectively, which, after being unified, agree well with each other. The material is found to follow a typical bilinear stress–strain relationship with an obvious plastic yielding but very slight hardening. Table 2 displays the mechanical properties of the material obtained from tests.

3. Experimental results and analysis

Test Set 1 (test nos. 1–5) was carried out for trial of the whole experimental set-up and Set 2 (test nos. 6–9) was for demo of the high-speed video camera which was newly installed. The remaining sets were tested in four groups with different focus: (1) the effect of the notch's presence, (2) the effect of increasing impact velocity, (3) the influence of notch width, and (4) the effect of notch location.

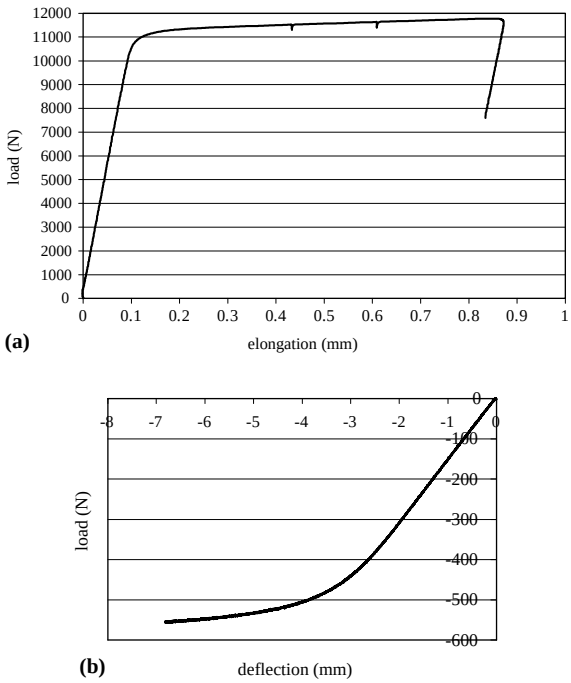

Fig. 5. Testing of material properties: (a) load-elongation diagram from simple tensile test and (b) loading-deflection diagram from three point bending test.

Table 2
Mechanical properties of specimen material

Young's modulus E (GPa)	Poisson's ratio v	Hardening modulus E_p (GPa)	Yield stress Y (MPa)	Peak stress σ_p (MPa)	Density ρ (kg/m^3)
68.95	0.33	0.466	277.8	292.0	2680

3.1. High-speed digital video photography

To gain real-time observation of the swift response and failure process of the beams after impact, in particular in the vicinity of the pre-notches, high-speed digital video photography was shot in 39 of our over 60 tests. As the entire process of each test lasted a few milliseconds only, we had to opt for a higher record rate (4000 frame/s) with a lower resolution of 100 98. The acquisitions were digital documents, which were stored and processed in the .avi format (movies) or in the .bmp format (frames of photos) on a PC. The .avi movies can be shown on PC screens, showing the dynamic response and failure (e.g. crack extension and breakage) scenarios of the tested specimens. Figs. 6–9 display the high-speed photographs in time-steps of 0.25 ms for four typical tests. No. 61 in Fig. 6 was a perfect (not pre-notched) specimen, which only underwent large plastic bending deformation after impact by a steel projectile (S1b) of 64 g travelling at $V_0 = 46.8$ m/s. With pre-notches, the other three beams that were subjected to impact of even lower velocities were either cracked or broken at the notched section (Figs. 7–9). A comparison in Table 3 reveals that the pre-notched beams are much easier to suffer a strength-failure (crack or break) than a perfect one.

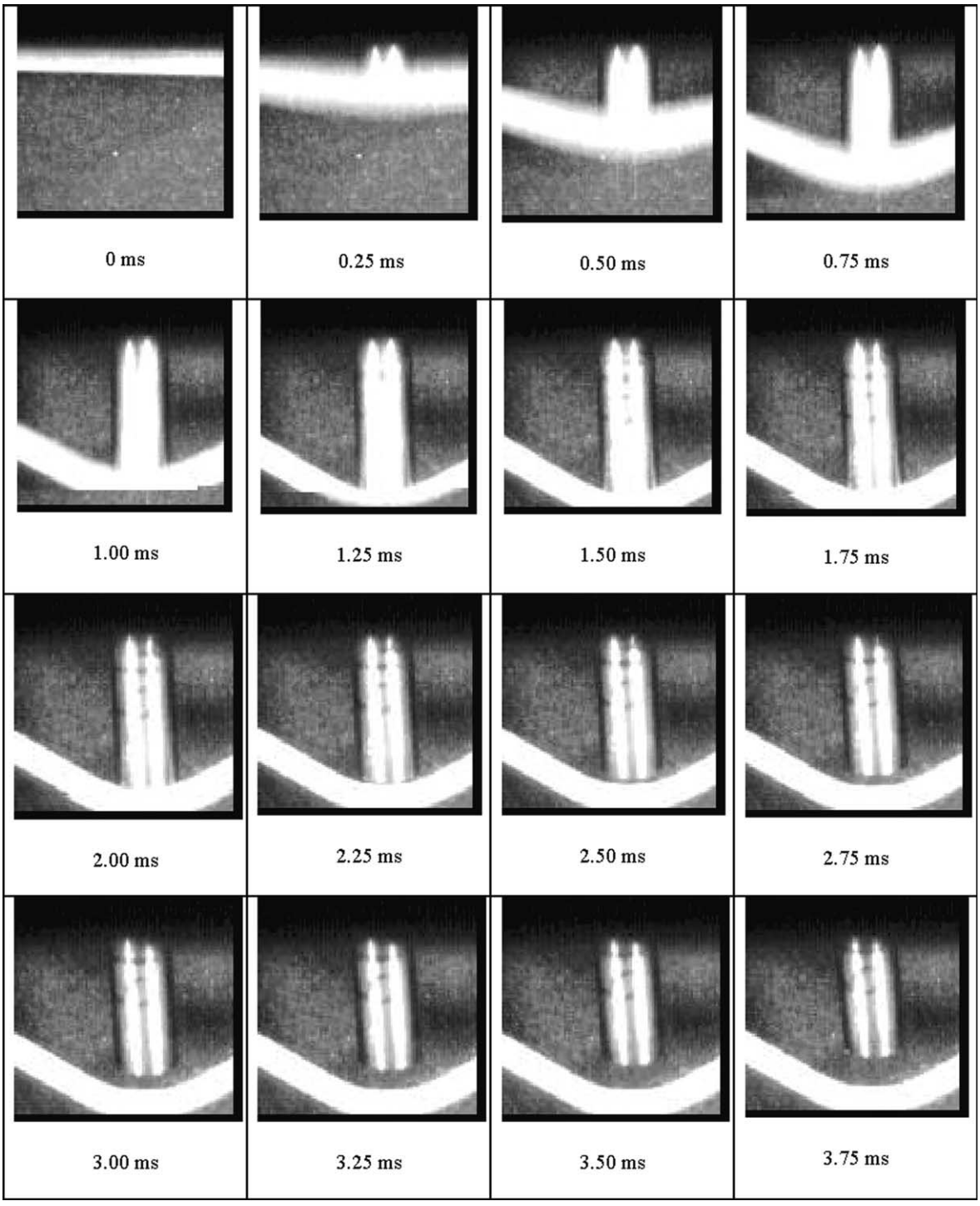

Fig. 6. High-speed photographs of perfect specimen no. 61 after impact ($G = 64$ g, $V_0 = 46.8$ m/s).

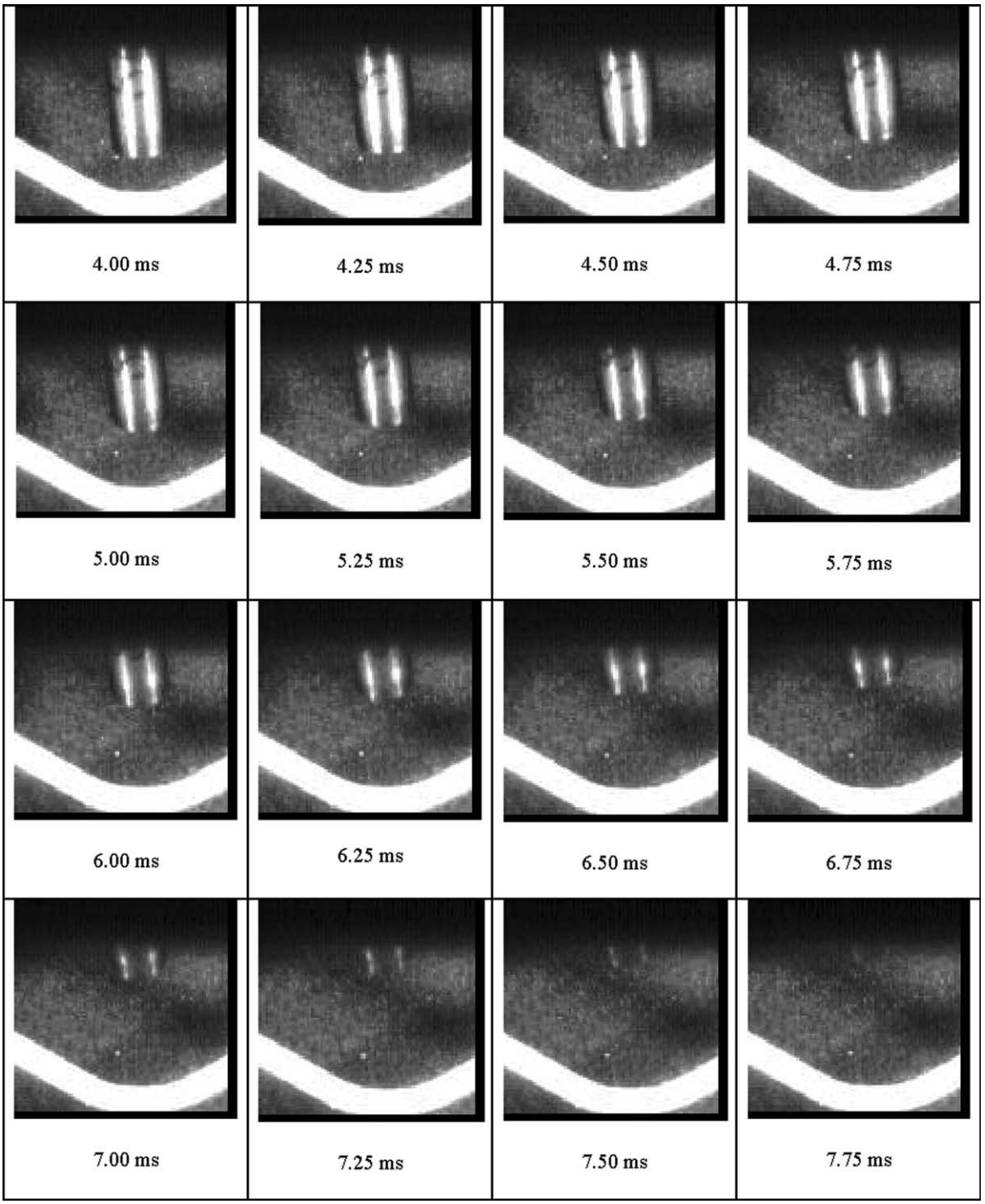

Fig. 6 *(continued)*

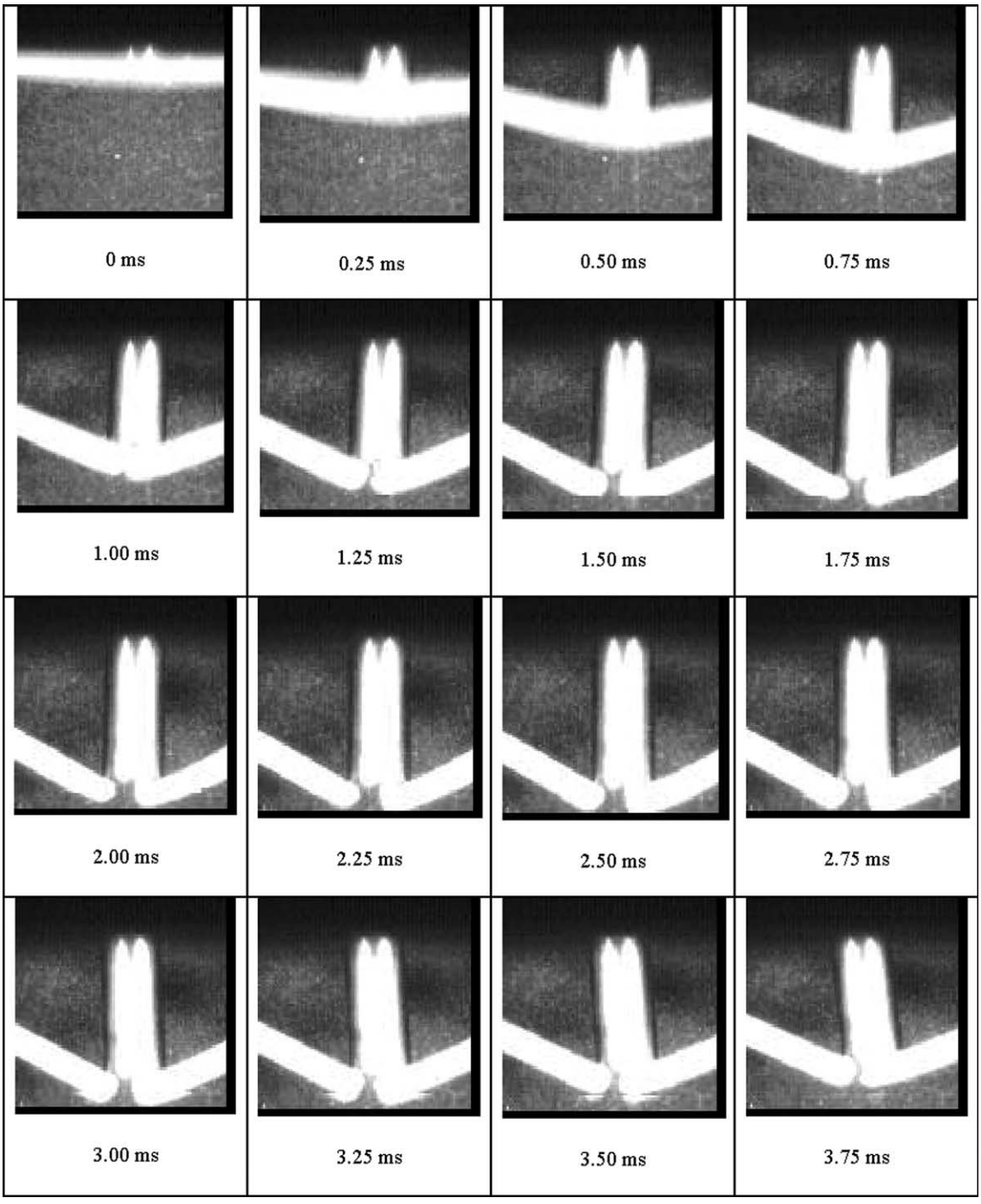

Fig. 7. High-speed photographs of slightly pre-notched specimen no. 59 after impact ($G = 64$ g, $V_0 = 35.0$ m/s).

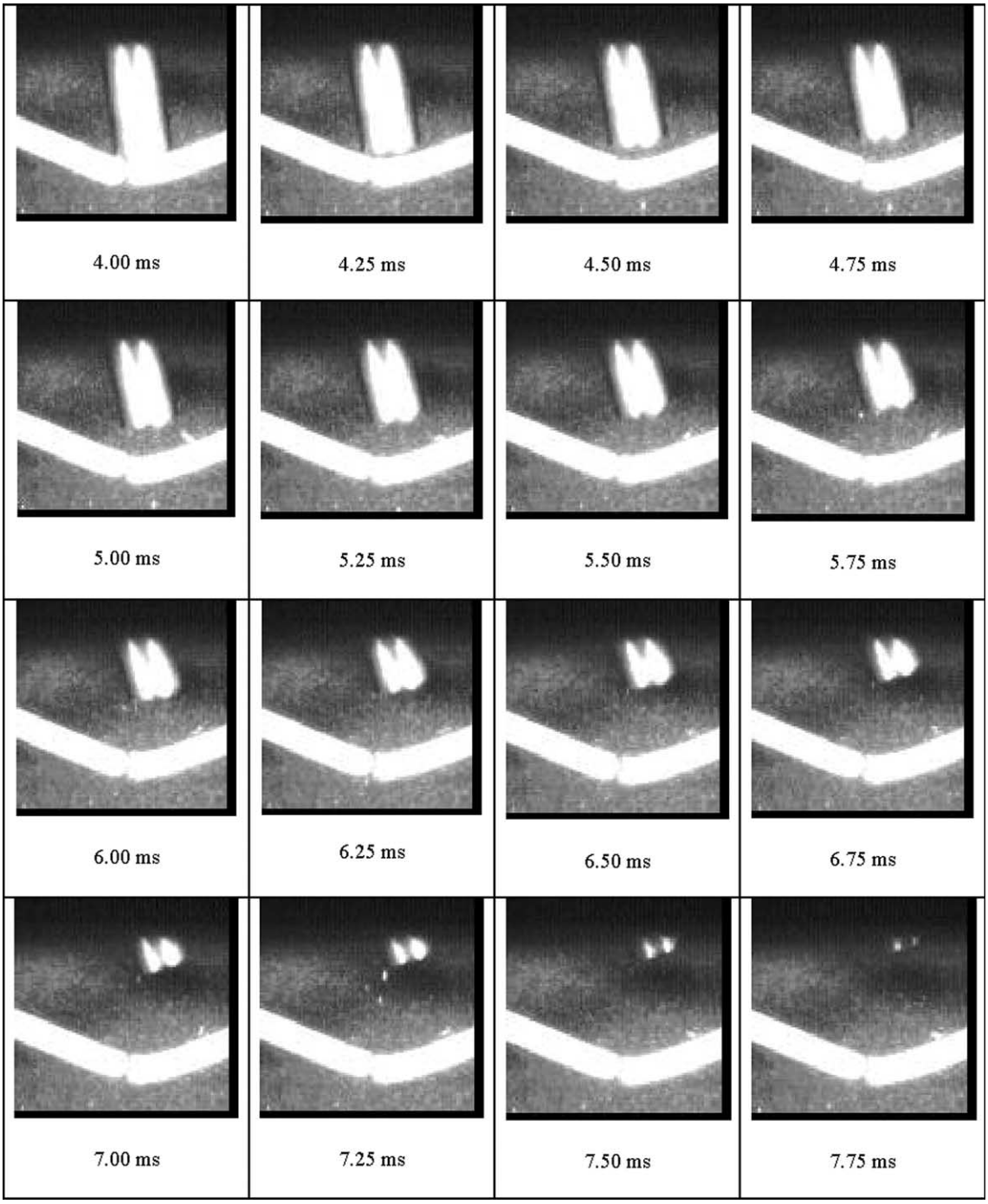

Fig. 7 *(continued)*

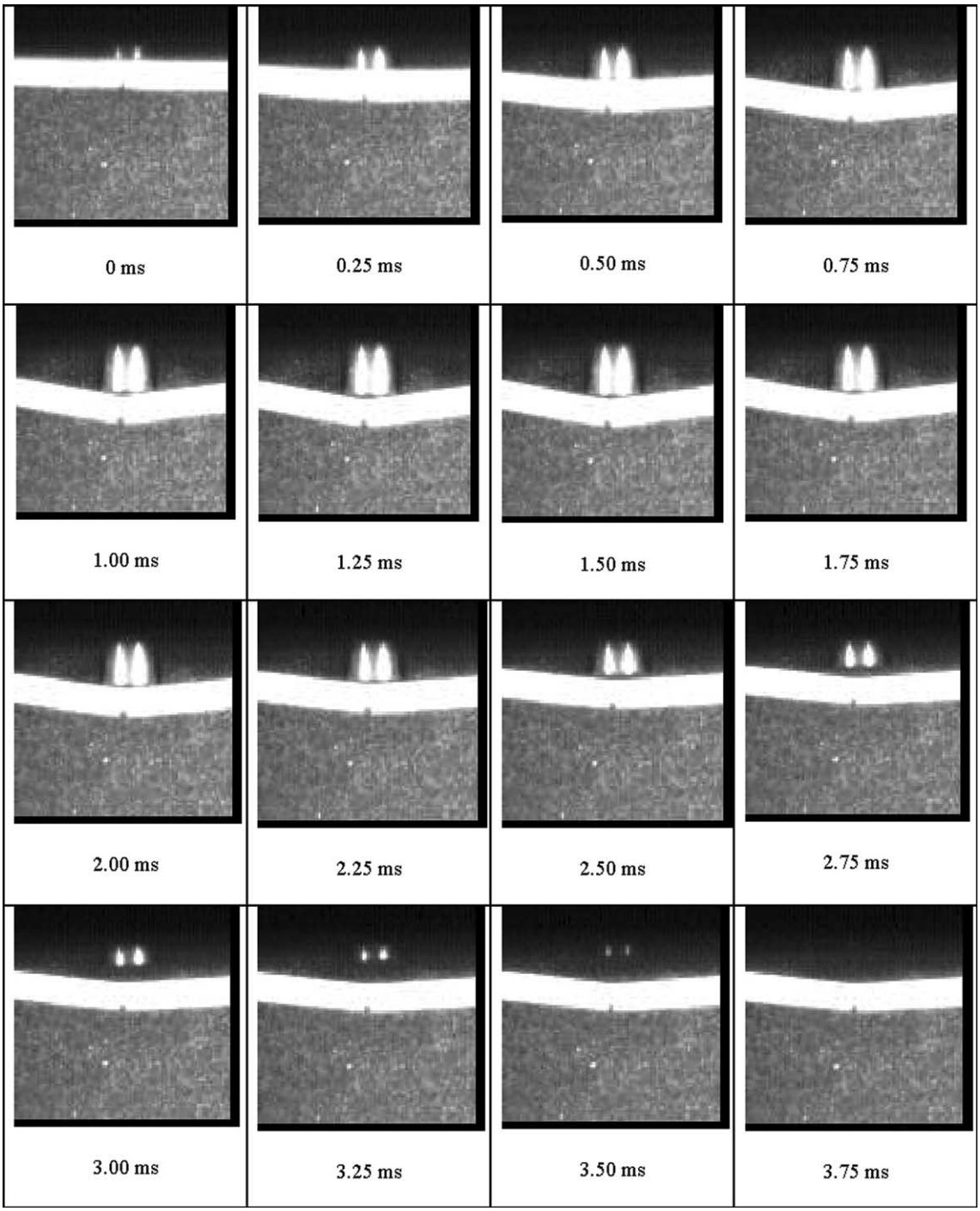

Fig. 8. High-speed photographs of sharply pre-notched specimen no. 56 after impact ($G = 64$ g, $V_0 = 15.7$ m/s).

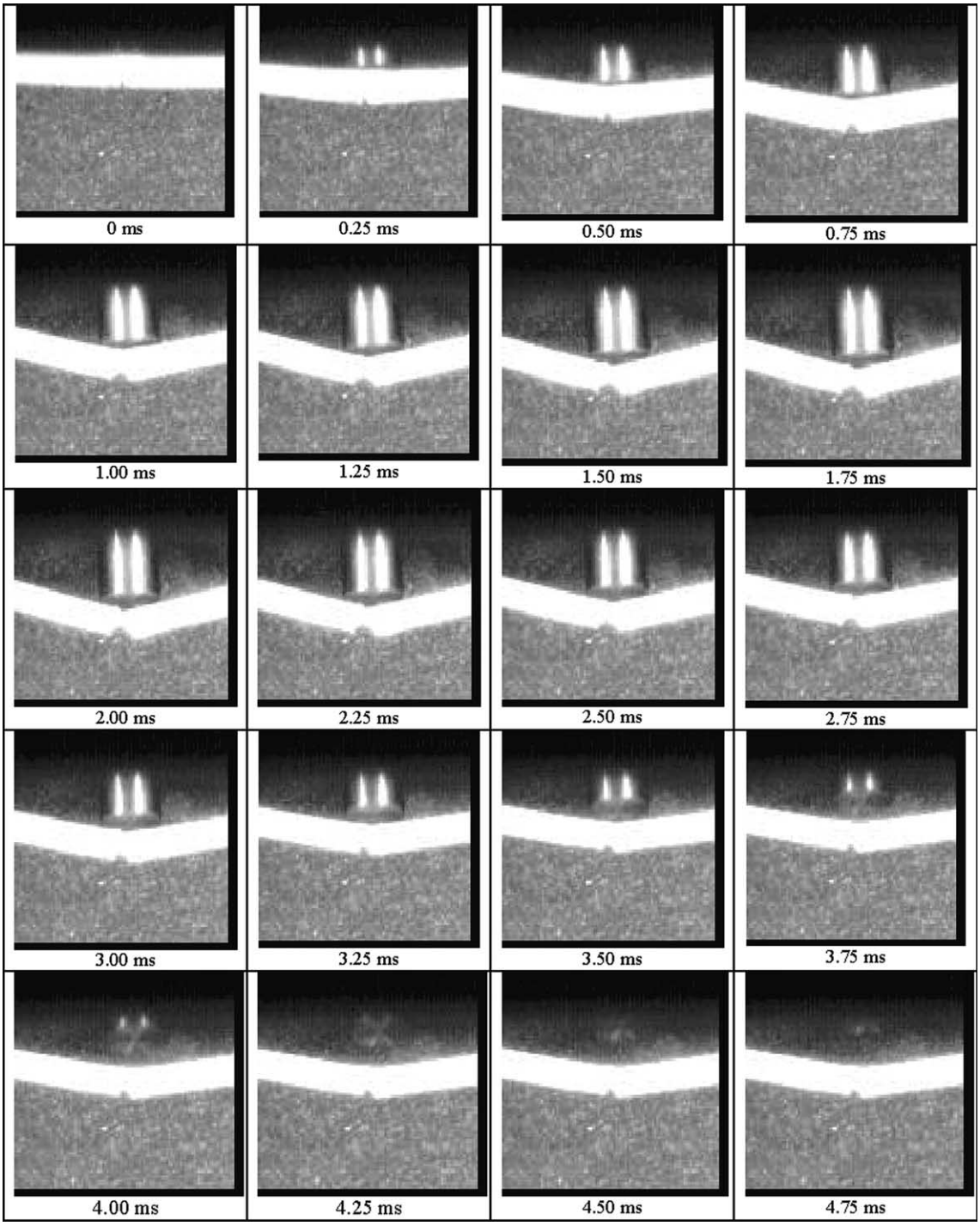

Fig. 9. High-speed photographs of sharply pre-notched specimen no. 55 after impact ($G = 64$ g, $V_0 = 20.0$ m/s).

Table 3
Analysis of high-speed photographs

Specimen no.		61 (Fig. 6)	59 (Fig. 7)	56 (Fig. 8)	55 (Fig. 9)
Notch	Depth C (mm)	–	0.85	2.12	
	Width (mm)	(perfect)	0.5	0.9 + sharp tip	
$\gamma = (1 - C/H)^2$		1	0.75	0.444	
S1b: G (g)		64.0	64.0	64.0	64.0
V_0 (m/s)		46.8	35.0	15.7	20.0
I_0 (N s)		3.00	2.24	1.00	1.28
t_b (ms)		–	1.25	1.25	1.50
t_s (ms)		1.50	2.50	1.25	1.75
t_r (ms)		2.25	4.25	2.75	3.00
$\bar{a}$ (g)		3184	1428	1282	1166
$\overline{F}$ (kN)		2.00	0.90	0.81	0.74
V_r (m/s)		4.23	5.08	5.08	4.23
K_r/K_0		0.82%	2.1%	10%	4.5%
$R = K_0/U^e_{max}$		29.2	16.3	3.29	5.33
$\lambda = K_0/M_0$		3.94	2.20	0.443	0.720
Dominant phenomenon		Large plastic bending deformation	Breakage at pre-notched section	2.7 mm-crack at pre-notched section	Just broke at pre-notched section

Note: $M_0 = \frac{1}{4} YBH^2 = 17.78$ Nm; $U^e_{max} = \frac{M_0^2(2EI)}{2EI} = 2.40$ J.

Table 4
Effect of the pre-notch's presence: Test Set 9 (Projectile: S1b)

No.	Notch location/f or b	Notch depth (mm)/width (mm)	Air pressure P (MPa)	Projectile velocity V_0 (m/s)	Projectile momentum I_0 (N s)	Observations	Maximum deflection W_{max} (mm)
57	No notch	–	0.40	57.9	3.71	Large plastic deformation; projectile rebounded	31.45
61	No notch	–	0.45	46.8	3.00	Large plastic deformation; projectile rebounded	32.10
60	(0L)[a]/b	0.90/0.5	0.20	28.4	1.82	Deformation, crack initiated, necking, no break; projectile rebounded	16.66
59	(0L)/b	0.85/0.5	0.25	35.0	2.24	Broken at notched section; projectile rebounded	23.28[b]
58	(0L)/b	0.85/0.5	0.35	49.4	3.16	broken at notched section; projectile penetrated	41.83[a]

Note (same in the following tables): f or b: on the front or back surface of the beam.
[a] In the bracket is the distance of the pre-notch from the mid-point of the beam.
[b] Nominal maximum deflection despite breakage of the beam.

Table 3 summarizes detailed analysis of these high-speed photographs, from which it is seen that

(1) the projectile was rebounded at time of 2.25–4.25 ms (refer to the analytical work by Schonberg et al. (1987));
(2) the average deceleration $\bar{a}$ before the projectile stops going ahead in the tests ranged from 1166g to 3184g, while the average impact force applied on the beam during the period, $\overline{F}$, ranged from 0.74

Fig. 10. Effect of notch's presence: Set 9 (nos. 57, 61, 60, 59, 58).

Table 5
Effect of increasing impact velocity: Test Set 4 (Projectile: S1b, S1c)

No.	Notch location/f or b	Notch depth (mm)/width (mm)	P (MPa)	V_0 (m/s)	I_0 (N s)	Observations	W_{max} (mm)
18	$(0L)/b$	2.12/1.25	0.075	15.2	0.97	Small plastic deformation, local necking, crack initiated; projectile rebounded	9.26
16	$(0L)/b$	2.12/1.25	0.10	17.2	1.10	Plastic deformation, local necking, short crack; projectile rebounded	10.99
15	$(0L)/b$	2.12/1.25	0.15	26.1	1.67	Broken at notched section; projectile rebounded	16.90[a]
14	$(0L)/b$	2.12/1.25	0.20	29.1	1.86	Broken at notched section; projectile rebounded	28.42[a]
19	$(0L)/b$	2.12/1.25	0.25	34.1	2.18	Broken at notched section; projectile rebounded	44.80[a]

[a] Nominal maximum deflection despite breakage of the beam.

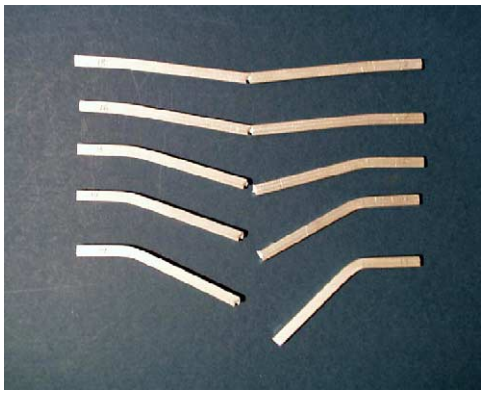

Fig. 11. Effect of increasing impact velocity: Set 4 (nos. 18, 16, 15, 14, 19).

Table 6
Effect of increasing impact velocity: Test Set 7a (Projectile: S1b)

No.	Notch location/f or b	Notch depth (mm)/width (mm)	P (MPa)	V_0 (m/s)	I_0 (N s)	Observations	W_{max} (mm)
26	$(-L, L)/f$	1.59/0.8	0.05	12.3	0.79	Small plastic deformation, small local necking; projectile rebounded	2.70
25	$(-L, L)/f$	1.59/0.8	0.10	18.5	1.18	Plastic deformation, local necking and cracks just initiated; projectile rebounded	7.55
24	$(-L, L)/f$	1.59/0.8	0.15	25.5	1.63	Large plastic deformation, large local necking and extended cracks; projectile rebounded	12.26
23	$(-L, L)/f$	1.59/0.8	0.20	30.3	1.94	Broken at notched ends; projectile rebounded	13.63[a]
22	$(-L, L)/f$	1.59/0.8	0.25	34.2	2.19	Broken at notched ends; projectile rebounded	15.53[a]
21	$(-L, L)/f$	1.59/0.8	0.30	41.5	2.66	Broken at notched ends; projectile rebounded	17.58[a]

[a] Nominal maximum deflection despite breakage of the beam.

Table 7
Effect of increasing impact velocity: Test Set 7b (Projectile: S1b)

No.	Notch location/f or b	Notch depth (mm)/width (mm)	P (MPa)	V_0 (m/s)	I_0 (N s)	Observations	W_{max} (mm)
32	$(-L, L)/f$	2.12/0.8	0.10	17.7	1.13	Small plastic deformation, local necking, cracks initiated; projectile rebounded	7.07
31	$(-L, L)/f$	2.12/0.8	0.15	24.7	1.58	Plastic deformation, large local necking, cracks occurred; projectile rebounded	13.03
30	$(-L, L)/f$	2.12/0.8	0.20	31.6	2.02	Broken at notched ends; projectile penetrated	13.73[a]
29	$(-L, L)/f$	2.12/0.8	0.25	33.8	2.16	Broken at notched ends; projectile penetrated	18.39[a]
28	$(-L, L)/f$	2.12/0.8	0.30	42.3	2.71	Broken at notched ends; projectile penetrated	16.77[a]

[a] Nominal maximum deflection despite breakage of the beam.

to 2.00 kN; if calibrated more precisely, the variation history with time of the deceleration of the projectile and impact force applied on the beam could be calculated from the displacements measured from the successive photographs;

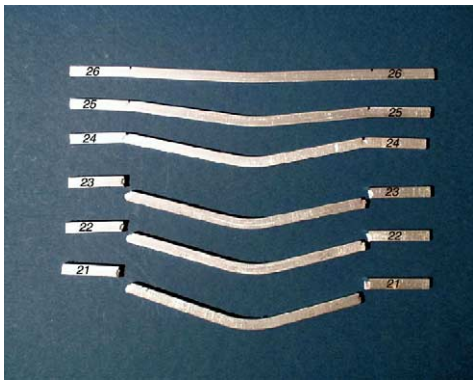

Fig. 12. Effect of increasing impact velocity: Set 7a (nos. 26, 25, 24, 23, 22, 21).

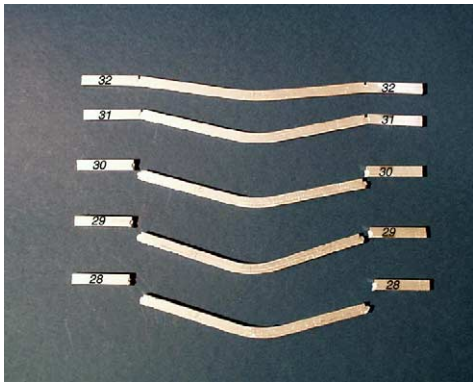

Fig. 13. Effect of increasing impact velocity: Set 7b (nos. 32, 31, 30, 29, 28).

(3) with the increase of energy ratio $R = K_0/U^{e}_{max}$ (here $K_0 = GV_0^2/2$ with G being mass of the projectile is the kinetic energy of the projectile before impact and $U^{e}_{max} = M_0^2(2L)/2EI = 2.40$ J is the maximum energy that the beam can store elastically), a larger portion of the projectile's initial kinetic energy was absorbed by the beam. For example, 95% of K_0 was absorbed by the beam if $R > 5$.

The photographs also show that springback due to elasticity of the tested beams were much less significant in comparison with the plastic deformation. The ratio of the kinetic energy taken away by the rebounded projectile to its initial kinetic energy, K_r/K_0, which always remains a small value in Table 3, is another index indicating the effect of elasticity. Therefore, the experimental evidences have justified the rigid-plastic idealization as a good approximation provided the energy ratio R is sufficiently large ($R > 5$, approximately).

Initially introduced by Petroski (1983), the reduced factor of a pre-notched beam can be defined as $\gamma = (1 - C/H)^2$ with C denoting the depth of notch. Although this reduced factor appropriately represents the effect of a notch in the global structural dynamic plastic response and energy distribution, it cannot be used to directly indicate the reduction in the capacity of a pre-notched beam to withstand impact loading. From perfect specimen no. 61 to pre-notched specimens no. 59, 56 and 55, γ reduces from 1 to 0.75 and 0.44 only, but the last two rows in Table 3 indicate that the beam's capacity of withstanding impact drops much

Table 8
Influence of notch width: Test Set 8 (Projectile: S1b)

No.	Notch location/f or b	Notch depth (mm)/width (mm)	P (MPa)	V_0 (m/s)	I_0 (N s)	Observations	θ_f (°)	W_{max} (mm)
52	$(0L)/b$	2.12/0.8	0.075	14.2	0.91	Local necking, crack initiated; projectile rebounded	12.5	7.92
54	$(0L)/b$	2.12/0.5	0.075	14.2	0.91	Local necking, shorter crack; projectile rebounded	12.7	7.61
56	$(0L)/b$	2.12/0.9 + sharp tip[a]	0.075	15.7	1.00	Local necking, longer crack; projectile rebounded	13.5	7.94
50	$(0L)/b$	2.12/1.5	0.10	19.2	1.23	Local necking, just broken; projectile rebounded	18.2[b]	10.18[b]
51	$(0L)/b$	2.12/0.8	0.10	18.2	1.16	Local necking, just broken; projectile rebounded	18.0[b]	8.62[b]
53	$(0L)/b$	2.12/0.5	0.10	19.5	1.25	Local necking, just broken; projectile rebounded	18.5[b]	8.63[b]
55	$(0L)/b$	2.12/0.9 + sharp tip[a]	0.10	20.0	1.28	Local necking, just broken; projectile rebounded	19.8[b]	10.08[b]
49	$(0L)/b$	2.12/1.5	0.15	27.1	1.73	Broken; projectile rebounded	29.8[b]	22.49[b]

[a] Half of the sharp tip angle was 45°. θ_f—the rotation angle at the pre-notched section.
[b] Nominal maximum deflection despite breakage of the beam.

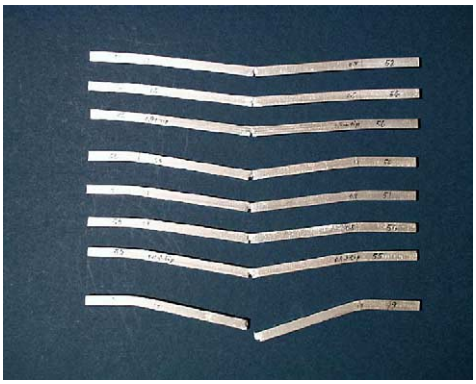

Fig. 14. Influence of notch width: Set 8 (nos. 52, 54, 56, 50, 51, 53, 55, 49).

more dramatically than the decrease rate in γ. For example, when $\gamma = 1$, the perfect specimen (no. 61) only experienced large plastic bending deformation under $R = 29.2$; when $\gamma = 0.75$ (i.e. it decreased by 25%), pre-notched specimen no. 59 broke at the pre-notched section under $R = 16.3$, and when γ decreases further to 0.44, pre-notched specimen no. 55 broke under $R = 5.33$. In short, a pre-notched structure is much more

vulnerable (especially in terms of strength-failure) than a perfect one. This point will be further elucidated in the following context.

3.2. Group 1: effect of notch's presence

Table 4 gives the test details of Set 9 (nos. 57, 61, 60, 59, 58). Specimens 57 and 61 were perfect, while specimens 60, 59 and 58 were machined with a minor pre-notch (depth $C \approx 0.85$ mm $= 0.13H$). Fig. 10 shows a comparison of the final shapes of the beams after impact. It is seen that the presence of the pre-notch resulted in (1) an evident concentration of plastic deformation and energy dissipation at the pre-notched section and the beam ends, (2) a much larger global deflection compared with a perfect

Table 9
Effect of notch location: Test Set 3 (Projectile: S1c)

No.	Notch location/f or b	Notch depth (mm)/width (mm)	P (MPa)	V_0 (m/s)	I_0 (N s)	Observations	W_{max} (mm)
10a	$(0L)/b$	2.12/1.25	0.30	41.1	2.63	Broken at notched section; projectile penetrated	37.8[a]
10b	$(0L)/f$	2.12/1.25	0.30	41.1	2.63	Notch closed; projectile rebounded	25.9
10	$(L/4)/f$	2.12/1.25	0.30	~41.1[b]	~2.63	Notch closed a little; projectile rebounded	22.2
11	$(L/2)/f$	2.12/1.25	0.30	~41.1	~2.63	No evident effect of notch; projectile rebounded	23.0
12	$(3L/4)/f$	2.12/1.25	0.30	~41.1	~2.63	Small local necking projectile rebounded	23.2
13	$(L)/f$	2.12/1.25	0.30	~41.1	~2.63	Broken at notched end; projectile rebounded	58.1[a]

[a] Nominal maximum deflection despite breakage of the beam.
[b] In test nos. 10–13, the projectile velocities were not measured, so 41.1 m/s was an approximate value.

Table 10
Effect of notch location: Test Set 5 (Projectile: A1a, A1b, A1c)

No.	Notch location/f or b	Notch depth (mm)/width (mm)	P (MPa)	V_0 (m/s)	I_0 (N s)	Observations	W_{max} (mm)
37	$(L/2)/f$	2.12/0.8	0.2	53.8	1.23	No evident effect of notch; projectile rebounded	15.50
39	$(3L/4)/f$	2.12/0.8	0.2	50.5	1.15	Small local necking at notch; projectile rebounded	15.94
41	$(L)/f$	2.12/0.8	0.2	55.1	1.26	Large local necking and short crack at notch; projectile rebounded	16.32

Table 11
Effect of notch location: Test Set 10 (Projectile: HS1a)

No.	Notch location/f or b	Notch depth (mm)/width (mm)	P (MPa)	V_0 (m/s)	I_0 (N s)	Observations	W_{max} (mm)
34	$(0L)/b$	2.12/0.8	0.30	34.5	2.92	Large local necking, broken at notched section; projectile penetrated	46.49[a]
36	$(L/4)/f$	2.12/0.8	0.30	30.4	2.57	Notch closed a little; projectile rebounded	20.88
38	$(L/2)/f$	2.12/0.8	0.30	31.1	2.63	No evident effect of notch; projectile rebounded	21.40
40	$(3L/4)/f$	2.12/0.8	0.30	38.1	3.22	Small local necking at notch; projectile rebounded	21.36
42	$(L)/f$	2.12/0.8	0.30	30.8	2.60	Large local necking, broken at notched end; projectile rebounded	59.09[a]

[a] Nominal maximum deflection despite breakage of the beam.

Fig. 15. Effect of notch location: Set 3 (nos. 10a, 10b, 10, 11, 12, 13).

counterpart, and (3) more prone to a strength failure at the pre-notched section. No strength failure took place in the perfect beam (no. 57) under impact of velocity of $V_0 > 57.9$ m/s, while a slightly pre-notched one experienced cracking even under impact of velocity 28.4 m/s (no. 60) but was utterly broken at $V_0 < 35.0$ m/s (no. 59). Note the input energy is proportional to the square of velocity.

It is thus concluded that even a minor pre-notch in a beam may dramatically alter its dynamic response and failure behavior and makes the beam much easier to break (i.e. switching from a large ductile plastic deformation to a local strength failure).

3.3. Group 2: effect of increasing impact velocity

All the specimens in Set 4 (nos. 18, 16, 15, 14, 19) were machined with a pre-notch (depth $C = H/3 = 2.12$ mm, width = 1.25 mm) on the back surface at the beam mid-section. By controlling the air

pressure in the air gun, the projectile velocity could gradually increase. Table 5 gives the test details of this set. Fig. 11 depicts a comparison of the final shapes of the beams of the set after impact. It is found that with increasing impact velocity, (1) the local plastic deformation (e.g. necking) increased gradually; (2) following large local plastic deformation (concentrated rotation and necking), a crack initiated as the impact velocity reached a certain level; (3) a longer crack occurred under larger impact velocities; and (4) when impact velocity reached another sufficient level V_c (between 17.2 and 26.1 m/s), the beam broke at the pre-notched section.

The specimens in sets 7a and 7b were all machined with two pre-notches on the front surface at the beam ends. The width of the notches was 0.8 mm; the notch depth for of Sets 7a and 7b was $C = H/4 = 1.59$ mm and $C = H/3 = 2.12$ mm, respectively. Tables 6 and 7 give the test details of the two sets, while Figs. 12 and 13 display the final shapes of the beams of these two sets after impact. The beam in Set 7a broke at a critical impact velocity $V_c < 30.3$ m/s (test no. 23), while the beam in Set 7b broke at critical impact velocity $V_c < 31.6$ m/s (test no. 30). It seems that the critical impact velocity for breakage at the pre-notched sections is not very sensitive to the depth of the pre-notch.

As observed in Sets 7a and 7b, as well as in Set 4, breakage was always found to take place at the pre-notched section. This again reflects the pronounced effect of the notches.

3.4. Group 3: influence of notch width

Test Set 8 (nos. 52, 54, 56, 50, 51, 53, 55, 49) was dedicated to exploring the influence of the notch width. The pre-notches machined on the beams had the same depth, but their width was taken to be 1.5, 0.8, 0.5 mm (a Π-shaped notch), and 0.9 mm with a sharp tip of angle 45°. Table 8 presents the test details for the set, while Fig. 14 exhibits the final shapes of the beams after impact. It is seen that the notch width has very minor influence on the final deflection of the beam and the rotation at the pre-notched section.

Comparing test nos. 52, 54 and 56, it is observed that the sharper was the notch tip (i.e. the smaller was the notch width), the longer was the crack extended. This in some degree reveals the influence of the width and the sharpness of the notch tip. However, the impact velocity required for breakage is found to be not very sensitive to the notch width. This point will be further elaborated in Section 3.6.

3.5. Group 4: effect of notch location

Test sets 3, 5, 10, 6a and 6b were designated to demonstrate how a pre-notch (or pre-notches) influences the dynamic response and failure of a beam. In Sets 3, 5 and 10, each specimen was machined with a pre-notch at a distance of $0L$ (mid-section), $L/4$, $L/2$, $3L/4$ or L (one end) away from the mid-section of the beam. The test details of these three sets are given in Tables 9–11, for which a steel projectile (Slc), three aluminium projectiles (A1a, A1b, A1c) and a high density steel projectile (HS1a) were respectively used. The final shapes of the beams are compared in Figs. 15–17.

The results have verified that the effect of pre-notch is highly location-dependent and surface dependent. A notch located at the impact point (nos. 10a, 13) or at one end of the beam (nos. 34, 42) led the beam to break at the pre-notched section; while a pre-notch located at $L/4$ or $3L/4$ only had a minor effect on the final shape, and that located at $L/2$ had an even negligible effect. The impact point and the beam's ends (or more generally, the positions where plastic hinges appear in a modal response of the beam) were found to be the most dangerous positions in the case of a large mass ratio $\beta = G/(2\rho BHL)$.

Comparing test nos.10a and 10b, it is found that a pre-notch located on the tensile surface of the beam has a much greater influence than that on the compressive surface. In the former case, the beam was utterly broken at the pre-notched section, while in the latter case, the pre-notch was only closed a little.

For test nos. 10, 11 and 12 of Table 9 and 36, 38 and 40 of Table 11, in spite of using different projectiles (64 and 84.5 g) and different velocities, the moment of the projectile, I_0 is almost the same, ~2.63. Then if

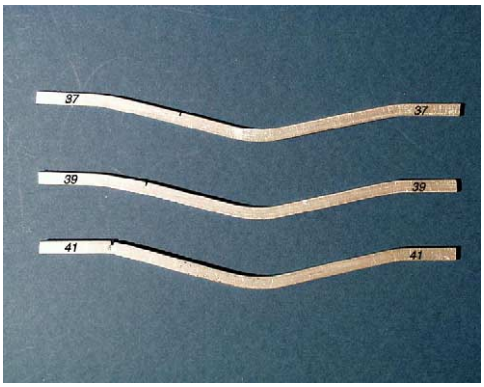

Fig. 16. Effect of notch location: Set 5 (nos. 37, 39, 41).

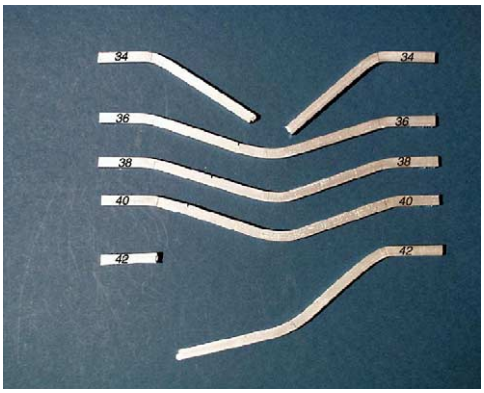

Fig. 17. Effect of notch location: Set 10 (nos. 34, 36, 38, 40, 42).

looking simultaneously at Figs. 14 and 16, we can see similar response patterns of the beam specimens in the different sets. The reason is that same moment of projectile will exert same impulse on the specimens, although the profile of the impulsive force is under the influence of many other factors.

In Sets 6a and 6b (Tables 12 and 13), each specimen was machined with two pre-notches located symmetrically at the two sides of the mid-point with distance of $\pm L/4$, $\pm L/2$, $\pm 3L/4$ or $\pm L$ away from there. The tests of these two sets used the air pressure of 0.30 and 0.35 MPa, respectively. It is seen from Figs. 18 and 19 that only the beam with pre-notches at two ends (no. 27) broke after impact by a steel projectile S1b travelling with initial velocity of 38.5 m/s; while all other beams with pre-notches elsewhere did not break even under higher impact velocities (Set 6b).

3.6. Local behaviour and broken surface

Fig. 20 shows close-up views of the local deformation (concentrated rotation and necking), crack or breakage at the pre-notched sections. The shapes of the local large deformation zones were of width 3–5 mm, and of a shape similar to the slip-line field of a pre-notched specimen. The size of the local deformation concentration zones is found to be not very sensitive to the width (and the tip-sharpness) of the pre-notches. This is because for sharp pre-notches (nos. 56 and 55), the notch tip blunted before a crack originated from there, while for Π-shaped notches, a crack originated from one of the notch corners. The effects of the

Table 12
Effect of notch location: Test Set 6a (Projectile: S1b)

No.	Notch location/f or b	Notch depth (mm)/width (mm)	P (MPa)	V_0 (m/s)	I_0 (N s)	Observations	W_{max} (mm)
43	$(-L/4, L/4)/f$	2.12/0.8	0.30	37.3	2.39	Plastic bending deformation, notches closed a little; projectile rebounded	21.44
45	$(-L/2, L/2)/f$	2.12/0.8	0.30	40.4	2.59	Plastic bending deformation, no evident effect of notches; projectile rebounded	23.80
47	$(-3L/4, 3L/4)/f$	2.12/0.8	0.30	41.8	2.68	Plastic bending deformation, small local necking at notches; projectile rebounded	24.57
27	$(-L, L)/f$	2.12/0.8	0.30	38.5	2.46	Plastic bending deformation, large local necking and broken at notched ends; projectile penetrated	17.57[a]

[a] Nominal maximum deflection despite breakage of the beam.

Table 13
Effect of notch location: Test Set 6b (Projectile: S1b)

No.	Notch location/f or b	Notch depth (mm)/width (mm)	P (MPa)	V_0 (m/s)	I_0 (N s)	Observations	W_{max} (mm)
44	$(-L/4, L/4)/f$	2.12/0.8	0.35	43.7	2.80	Large plastic bending, notches closed a little; projectile rebounded	28.45
46	$(-L/2, L/2)/f$	2.12/0.8	0.35	42.7	2.73	Large plastic bending, no evident effect of notches; projectile rebounded	27.96
48	$(-3L/4, 3L/4)/f$	2.12/0.8	0.35	41.1	2.63	Large plastic bending, small local necking at notches; projectile rebounded	28.30

relevant factors on the local behavior at the pre-notches, as discussed above, can be clearly seen from these photos.

Fig. 21 shows the broken surfaces of two typical specimens (nos. 59 and 55). It is found that only the broken surfaces of the specimen with a minor pre-notch (no. 59) were somewhat rough, while the broken surfaces of the other specimen with deeper pre-notches (e.g. no. 55) were flat and developed in the transverse direction. This implies that in most cases the breakage was basically caused by a Mode I crack

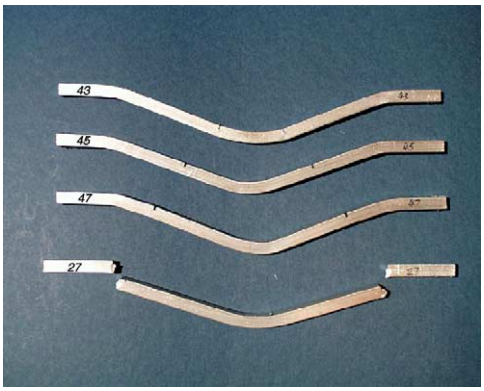

Fig. 18. Effect of notch location: Set 6a (nos. 43, 45, 47, 27).

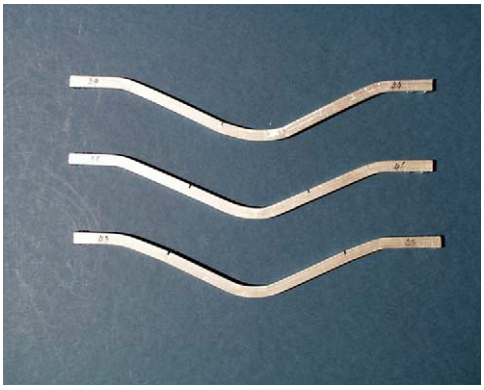

Fig. 19. Effect of notch location: Set 6b (nos. 44, 46, 48).

extension (failure Mode V), rather than by a shear sliding at 45° (failure Mode IV) as observed by Liu and Jones (1987) in their experiments on perfect clamped beams. This is one of our important experimental findings.

4. Comparison with theoretical predictions

Fig. 22 shows a comparison of the maximum deflection measured from test Sets 7a and 7b to the predictions obtained from a complete rigid-plastic (R-P) analysis (Chen and Yu, 1999) where no material failure (crack initiation and extension) is allowed to take place. They are found in favorable agreement with each other, which justifies the rationality of the rigid-plastic (R-P) analysis when the energy ratio R is large. It is also noted that the R-P analytical results are slightly larger than the experimental measurements. This could be attributed to the assumption in the R-P analysis that all the initial kinetic energy of the projectile is absorbed by the plastic deformation of the beam. In the experiments, however, the elastic deformation of the beam, the rebound of the projectile, and the crack extension (if occurs) all account for some non-negligible fractions of the energy consumption.

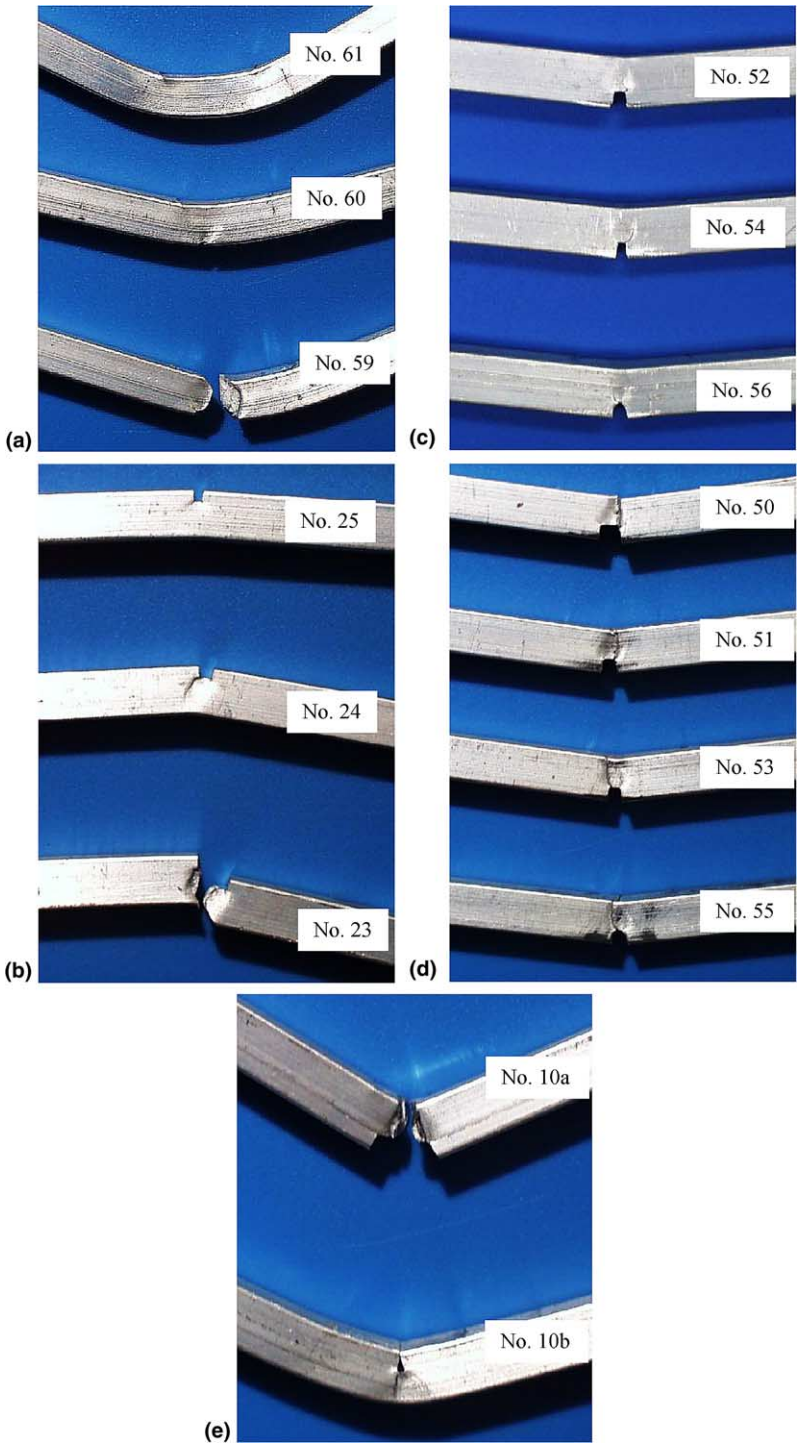

Fig. 20. Close-up views of local deformation (necking), crack and breakage at notched sections. (a) Large global deformation (bending) of a perfect specimen and local deformation (necking), crack and breakage at pre-notched sections of imperfect specimens. (b) Short crack, long crack and breakage at notched supporting (left) end: effect of increasing impact velocity. (c) Local necking and cracks: influence of notch width ($P = 0.075$ MPa). (d) Local necking and broken: influence of notch width ($P = 0.10$ MPa). (e) Broken and notch closed: surface dependent effect of pre-notch.

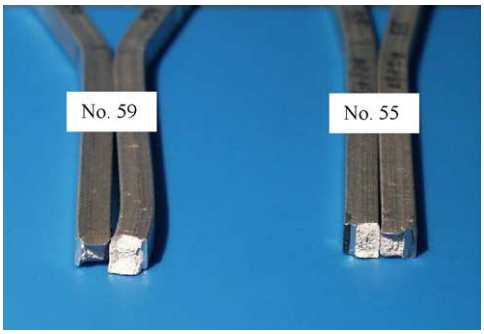

Fig. 21. Broken surfaces (notch depth was $0.13H$ and $H/3$, respectively).

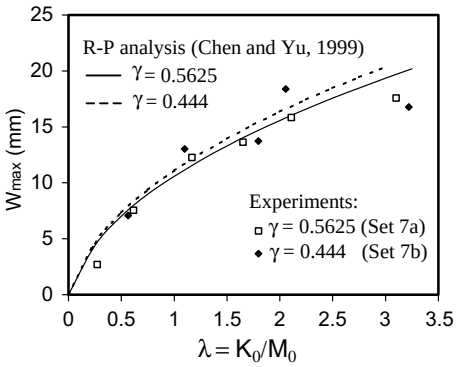

Fig. 22. Comparison of experiments with theoretical analysis (Chen and Yu, 1999) on the maximum deflection $W_{\max}$.

5. Conclusions

(1) The presence of a pre-notch or pre-notches in a clamped beam dramatically alters its dynamic failure behavior. The experiment reveals that pre-notched beams are much more likely to suffer a strength-failure (crack or break) than the perfect counterparts.

(2) The effect of a pre-notch is strongly location-dependent and surface-dependent. The mid-section and two ends of a clamped beam are the most dangerous positions, $L/4$ and $3L/4$ are less sensitive and $L/2$ is an insensitive position. A notch/crack on the tensile-surface of the beam under bending has a larger influence than one on the compression surface.

(3) A pre-notch located at a sensitive position of the beam makes the plastic deformation and plastic dissipation much more concentrated at the pre-notched section, which is demonstrated by (i) a large rotation angle at the pre-notched section in between two straight neighboring segments owing to the "shelter effect", and (ii) an evident local necking at the pre-notched section. Thus, a pre-notch usually makes the beam much more easily to be cracked or broken at the pre-notched section (failure Mode V) instead of other competitive failure mechanisms. Although the reduced factor defined by $\gamma = (1 - C/H)^2$ appropriately represents the effect of a notch in the global structural dynamic plastic response and energy distribution, it cannot be used to directly indicate the reduction in the capacity of a notched structure to withstand impact loading.

(4) If impact velocity or input energy is small, only concentrated plastic deformation occurs at the pre-notched section. With the increase of impact velocity or input energy, a crack initiates and propagates, and finally leads to breakage at the pre-notched section when the impact velocity or input energy reaches a sufficient level. The occurrence of crack propagation is always accompanied by a large local plastic deformation (concentrated rotation and necking).
(5) The sharper is the pre-notch tip, the more concentrated at the crack tip the plastic deformation and dissipation, and the more easily the crack initiates and propagates. However, for a Π-shaped notch, the threshold impact velocity (or energy) required for occurrence of breakage is not very sensitive to the notch width since the crack is only initiated at a corner of the notch width. The breakage is caused basically by a Mode I crack extension.

Acknowledgements

The work described in this paper was conducted as part of CERG research project HKUST811/96E and HKUST6035/99E funded by the Hong Kong Research Grant Council (RGC). The authors wish to express their gratitude to this support.

References

Chen, F.L., Yu, T.X., 1999. Dynamic behavior of a clamped plastic beam with cracks at supporting ends under impact. ASCE J. Pres. Ves. Tech. 121, 406–412.
Jones, N., 1976. Plastic failure of ductile beams loaded dynamically. Trans ASME J. Eng. Ind. 98 (B1), 131–136.
Jones, N., 1989. On the dynamic inelastic failure of beams. In: Wierzbicki, T., Jones, N. (Eds.), Structural Failure. John Wiley, New York, pp. 133–159.
Li, Q.M., Jones, N., 2000. Formation of a shear localization in structural elements under transverse dynamic loads. Int. J. Solids Struct. 37, 6683–6704.
Liu, J.H., Jones, N., 1987. Experimental investigation of clamped beams struck transversely by a mass. Int. J. Impact Eng. 6, 303–335.
Liu, J.H., Jones, N., 1988. Dynamic response of a rigid plastic clamped beam struck by a mass at any point on the span. Int. J. Solids Struct. 24, 251–270.
Menkes, S.B., Opat, H.J., 1973. Broken beams. Exp. Mech. 13, 480–486.
Nonaka, T., 1967. Some interaction effects in a problem of plastic beam dynamics, Parts 1–3. ASME J. Appl. Mech. 34, 623–643.
Petroski, H.J., 1983. Structural dynamics of piping with stable cracks: some simple models. Int. J. Pres. Ves. Piping 13, 1–18.
Petroski, H.J., Verma, A., 1985. Plastic response of cantilevers with stable cracks. ASME J. Eng. Mech. 111, 839–853.
Schonberg, W.P., Keer, L.M., Woo, T.K., 1987. Low velocity impact of transversely isotropic beams and plates. Int. J. Solids Struct. 23, 871–896.
Shen, W.Q., Jones, N., 1993. Dynamic plastic response and failure of a clamped beam struck transversely by a mass. Int. J. Solids Struct. 30, 1631–1648.
Woodward, R.L., Baxter, B.J., 1986. Experiments on the impact bending of continuous and notched steel beams. Int. J. Impact Eng. 4 (1), 57–68.
Yang, J.L., Zhang, Y., Yu, T.X., 1992. An experimental study of imperfect clamped beams subjected to impact. Explosion Shock Waves 12, 22–29 (in Chinese).
Yu, J.L., Jones, N., 1991. Further experimental investigation on the failure of clamped beams under impact loads. Int. J. Solids Struct. 27, 1113–1137.
Yu, J.L., Jones, N., 1997. Numerical simulation of impact loaded steel beams and the failure criteria. Int. J. Solids Struct. 34, 3977–4004.
Yu, T.X., Chen, F.L., 2000a. Failure of plastic structures under intense dynamic loading: modes, criteria and thresholds. Int. J. Mech. Sci. 42, 1537–1554.
Yu, T.X., Chen, F.L., 2000b. A further study of plastic shear failure of impulsively loaded clamped beams. Int. J. Impact Eng. 24, 613–629.
Zhao, Y.P., Fang, J., Yu, T.X., 1995. Experimental and theoretical investigations into circular rings under impact loading. DYMAT J. 2, 135–142.